

# Relativistic Centrifugal Instability

Konstantinos N. Gourgouliatos\*

*Department of Applied Mathematics, University of Leeds, Leeds LS2 9JT, UK,  
Department of Mathematical Sciences, Durham University,  
Mountjoy Centre, Stockton Rd, DH1 3LE, Durham, UK*

Serguei S. Komissarov†

*Department of Applied Mathematics, University of Leeds, Leeds LS2 9JT, UK  
(Dated: June 6, 2022)*

Motivated by astrophysical relativistic jets with curved streamlines, we explore the onset and the evolution of the Relativistic Centrifugal Instability (RCFI). As a first step, we study axisymmetric rotating flows, where the density and angular velocity change discontinuously at a given radius. Following the original physical argument of Lord Rayleigh, we derive the relativistic version of the Rayleigh criterion for this problem and use axially symmetric computer simulations to verify its predictions.

Over the last few decades, various astronomical studies revealed that both relativistic and non-relativistic compact accreting cosmic objects often produce spectacular collimated outflows. The speeds of these jets range from  $100 \text{ km/s}$  in the case of jets associated with young stars [1], to almost the speed of light in the case of jets associated with Active Galactic Nuclei (AGN) [3], micro-quasars [12] and Gamma Ray Bursts [7]. The current models of the astrophysical jet production include a rapidly rotating central object and magnetic fields and predict that these jets are also rapidly-rotating close to their central engines. Detailed imaging of protostellar jets has already detected such rotation [8, 20]. Relativistic jets of AGN may develop curved streamline at much larger distances as well, where they are expected to change their propagation regime from freely expanding to confined by the pressure of external gas [13, 17]. Such jets may suffer the centrifugal instability (CFI).

Lord Rayleigh [16] demonstrated that the rotation of an axially symmetric incompressible and inviscid fluid is unstable provided

$$\frac{d\Psi}{dR} < 0, \quad (1)$$

where  $\Psi = (\Omega R^2)^2$  is known as the Rayleigh discriminant,  $\Omega$  is the angular velocity,  $R$  is the cylindrical radius. Bayly [2] has shown that the unstable modes can be highly localised near the streamlines where the Rayleigh condition is satisfied, thus increasing the significance of the Rayleigh instability criterion as a local condition. In particular, this condition is always satisfied, at least locally, if  $\Omega$  vanishes at some radius. For example, in curved pipe flows the fluid comes to rest within a boundary layer. This leads to the phenomenon of Görtler vortices [4], which may trigger turbulent cascade and disrupt the flow [18]. In the case of reconfined jets a similar configuration emerges because the external medium is at rest and the jet boundary is concave.

In the case of astrophysical jets, not only the velocity but also mass density are expected to show significant variation across the jets. In addition, these jets are mostly supersonic and hence one has to allow for fluid compressibility. Finally,

the structure of reconfined jets is rather complicated. In order to reduce the level of complexity and allow clear-cut conclusions we investigate a rotating unmagnetised relativistic fluid. We focus on the case where the instability is produced by a jump of the physical parameters at a given radius, reflecting the strong contrast between the jet and its environment.

*Generalised Rayleigh Criterion.* The energy-momentum equation of relativistic hydrodynamics can be written as

$$\rho \frac{Dhu_\mu}{D\tau} = -\frac{\partial p}{\partial x^\mu} - \frac{p}{\sqrt{|g|}} \frac{\partial \sqrt{|g|}}{\partial x^\mu} - \frac{1}{2} T^{\alpha\beta} \frac{\partial g_{\alpha\beta}}{\partial x^\mu}, \quad (2)$$

where  $T^{\alpha\beta} = wu^\alpha u^\beta + g^{\alpha\beta}$  is the stress-energy-momentum tensor,  $g^{\alpha\beta}$  the metric tensor and  $g$  its determinant,  $w = e + p$  the relativistic enthalpy per unit volume and  $h = w/\rho$  the enthalpy per unit mass,  $e$  the internal energy density,  $\rho$  the rest mass density,  $p$  the pressure and  $u^\mu$  the 4-velocity vector of the fluid.  $D/D\tau$  is the absolute derivative along the world-lines of fluid elements. We use natural units so that  $c = 1$ . In Minkowski space-time with cylindrical spatial coordinates  $\{z, R, \phi\}$ , the azimuthal component of equation 2 reads

$$\frac{D(hu_\phi)}{D\tau} = 0, \quad (3)$$

where  $u_\phi = \Gamma\Omega R^2$ . This constitutes the angular momentum conservation law. The radial component reads

$$\rho \frac{D(hu_R)}{D\tau} = -\frac{\partial p}{\partial R} + \frac{wu_\phi^2}{R}, \quad (4)$$

where  $u_\phi = \Gamma\Omega R$  is the azimuthal component of the 4-velocity in the normalised coordinate basis. In equilibrium, the radial force vanishes

$$f_R = -\frac{\partial p}{\partial R} + \frac{wu_\phi^2}{R} = 0. \quad (5)$$

First we deal with an equilibrium involving a tangential discontinuity at  $R = R_d$ . Denote the fluid parameters just below

and above  $R_d$  using suffices “1” and “2” respectively. Following the Rayleigh argument, we consider a fluid ring pushed upwards across the discontinuity. After the crossing, it will be subject to the force

$$f_R^* = -R_d[\bar{\Psi}], \quad (6)$$

where  $\bar{\Psi} = w(\Gamma\Omega)^2$  and we denote  $[Q] = Q_2 - Q_1$  for some quantity  $Q$ . The force will push the ring further up provided

$$[\bar{\Psi}] < 0, \quad (7)$$

which is the instability condition for the discontinuity. In the Newtonian limit  $\bar{\Psi} = \rho\Omega^2$ .

When  $\Omega$  is continuous across the discontinuity the criterion reduces to  $[\Gamma^2 w] < 0$  which reads  $[\rho] < 0$  in the Newtonian limit. Such a configuration can be regarded as the one of the Rayleigh-Taylor instability [15, 19], with the centrifugal force playing the role of gravity. Both the reduced instability criteria state that the configuration is unstable when a fluid of higher inertial mass density is placed on top of a lighter fluid.

Now consider the case of continuous variation of parameters. This time a fluid ring is displaced from  $R = R_1$  to  $R = R_2 = R_1 + \delta R$ . Without loss of generality we may assume that  $\delta R > 0$ . After the displacement the force acting on the ring is

$$f_R^* = -\frac{1}{R_2} \left( w_2(u_{2,\phi})^2 - \tilde{w}_1(\tilde{u}_{1,\phi})^2 \right) = 0, \quad (8)$$

where  $\tilde{q}_1 = q_1 + \delta q$  indicates the value of quantity  $q$  after the displacement. For adiabatic motion  $\delta e = h\delta\rho$  and  $\delta\rho = \delta P/ha^2$ , where  $a$  is the sound speed. Combining these equations with the Eq. (5) we find

$$\frac{\delta\rho}{\rho_1} = \frac{u_{1,\phi}^2}{a_1^2} \frac{\delta R}{R_1} \quad (9)$$

and

$$\frac{\delta w}{w_1} = \left( \frac{1 + a_1^2}{a_1^2} \right) u_{1,\phi}^2 \frac{\delta R}{R_1}. \quad (10)$$

To find the variation of the velocity, we combine the angular momentum conservation  $h_1 u_{1,\phi} R_1 = \tilde{h}_1 \tilde{u}_{1,\phi} R_2$  with the above results for the thermodynamic parameters to obtain

$$\tilde{u}_{1,\phi} = u_{1,\phi} \frac{R_1}{R_2} \left( 1 - u_{1,\phi} \frac{\delta R}{R_1} \right). \quad (11)$$

Substituting the results into Eq. (8) we find that the displaced ring will be pushed further up provided

$$\frac{d \ln \Psi}{d \ln R} < M^2, \quad (12)$$

where

$$\Psi = w\Gamma^2(\Omega R^2)^2 \quad (13)$$

Run	$\rho_1$	$\rho_2$	$\Omega_1$	$\Omega_2$	$p(1)$	$\Delta\hat{\Psi}$	Stability
R1	1	1	0.9	0	284	-2.00	U
R2	1	1	0.9	0.45	284	-1.76	U
R3	1	2	0.45	0.45	16	0.51	S
R4	2	1	0.45	0.45	16	-0.02	B
C1	1	1	2	1	12	-1.19	U
C2	2	1	2	1	14	-1.55	U
C3	1	2	2	1	12	-0.65	U
C4	1	2	1	1	10.5	0.68	S
C5	2	1	1	1	11	-0.65	U
C6	2	1	1	2	11	0.68	S

TABLE I. Simulation models. The first column is the model name, C denotes the newtonian runs and R the relativistic ones. The second to fifth columns contain the density and angular momentum of the inner and outer fluid. The sixth is the relative change of the Rayleigh discriminant at the interface  $\Delta\hat{\Psi} = [\bar{\Psi}]/\langle\Psi\rangle$ . The last column shows if the initial configuration is found to be stable (S) or unstable (U). In the model R4 the growth rate of the instability is very slow; it is saturated at a rather small amplitude and eventually damped by numerical dissipation. For this reason it is marked as a borderline case (B).

is the generalised Rayleigh discriminant and  $M = \Gamma v_\phi/\Gamma_a a$  is the relativistic Mach number of the rotational motion.

When expressed in terms of a finite jump the criterion (12) is fully consistent with (7) for a discontinuity. In the Newtonian limit, the instability criterion has the same form as (12) but with  $M = v/a$  and

$$\Psi = \rho(\Omega R^2)^2. \quad (14)$$

Furthermore, in the incompressible limit,  $M = 0$  and  $\rho = \text{const}$ , we recover the original Rayleigh criterion.

*Setup of Computer Simulations.* To verify the instability criterion we carry out computer simulations for the configuration where the axial velocity  $v_z = 0$  and both the density and the angular velocity are piecewise constant:

$$\rho, \Omega = \begin{cases} \rho_1, \Omega_1 & R \leq 1, \\ \rho_2, \Omega_2 & R > 1. \end{cases} \quad (15)$$

The pressure distribution is derived using the equilibrium Eq. (5), and is determined with a freedom of an integration constant. We determine this constant by setting the pressure on the axis  $p(0) = 10$  for all simulations. The parameters chosen for these runs are shown in Table 1. According to the criterion (12) the configuration is stable on both sides of the discontinuity and hence the stability of the whole configuration is determined by the criterion (7) for the discontinuity.

We have chosen the angular velocity of the relativistic runs (R1-R4) so that the maximum velocity of the flow does not exceed  $0.9c$ . All our simulations are two-dimensional with imposed axial symmetry. For the sake of comparison between the relativistic and Newtonian systems, we have also carried

out non-relativistic runs for similar configurations. We used the AMRVAC code; the HD module for the classical case and the SRHD module for the relativistic one [6, 14]. To track the fluids initially located at either side of the discontinuity, we used a passive tracer  $\eta$  satisfying the following equation

$$\partial(\Gamma\rho\eta)/\partial t + \nabla \cdot (\Gamma\rho\eta\mathbf{v}) = 0,$$

( $\Gamma$  is set to unity for the non-relativistic case). It is initialised so that  $\eta = 1$  for  $R < 1$  and  $\eta = 0$  for  $R > 1$ . The computational domain is  $(R, z) \in (0, 2) \times (0, 2)$  with a uniform  $400 \times 400$  grid. At  $R = 0$  we use the reflection boundary conditions and at  $R = 2$  we use symmetry conditions for  $\rho$ ,  $p$ ,  $v_\phi$  and  $v_z$  and the anti-symmetry condition for  $v_R$ . The initial equilibrium configuration was perturbed via a sinusoidal perturbation of the azimuthal velocity component in the vicinity of  $R = 1$ , with wavenumber  $k = 5$  and amplitude  $10^{-3}$  of the local azimuthal velocity. In order to test the convergence, we made some runs with double resolution. This resulted to the emergence of finer features but the overall evolution remained unchanged.

*Simulation Results.* As summarised in table I, the results of our simulations are in complete agreement with the generalised Rayleigh criterion (7), both in the Newtonian and relativistic regimes. In particular, the relativistic models R1 and R2, where the initial density is uniform but the angular velocity on the outside of the discontinuity is smaller than on the inside, are unstable. The relativistic models R3 and R4 have uniform rotation and hence their initial configuration is analogous to the one of the Rayleigh-Taylor problem. The model R3 has a lighter fluid on the inside of the discontinuity and it is stable whereas the model R4 has a heavier fluid on the inside and it is unstable, as expected. Among the unstable models, by the end of the simulations the model R1 is totally disrupted (see Figure 1), R2 develops a turbulent layer around the discontinuity but retains mostly undisturbed inner and outer regions and R4 shows very early saturation of the instability. This is illustrated in the left panel of figure 2 which shows the final distribution of the passive tracer. These outcomes allow a simple interpretation: As the instability enters the nonlinear phase it begins to modify the spatial distribution of the generalised Rayleigh discriminant by reducing the size of region where the instability criterion is satisfied (see the right panel of Figure 2). In the model R4, where the jump of  $\Psi$  is very small, such a region is completely erased even before the instability reaches high amplitude. In the model R2, where the jump is almost one hundred times larger, this occurs much later. Finally, in the model R1 the instability criterion is satisfied all the time because the undisturbed external fluid is at rest.

The same behaviour is observed for the Newtonian models (see C-models in Table I and Figures 3 and 4). In particular, a higher jump of the generalised Rayleigh discriminant leads to a more disturbed final solution. Models C3 and C5 have rather different jumps of density and angular velocity but the same jump of the discriminant and develop turbulent layers of

similar size (see figure 4). The initial configurations of C4 and C5 are analogous to that of the Rayleigh-Taylor problem and show that in this case the instability develops only when the inner fluid is heavier, as expected for RTI. In the model C3, the inner fluid is lighter but the instability still develops because the jump of the angular velocity ensures that the Rayleigh criterion for CFI is satisfied.

The common feature of the nonlinear phase of CFI in all our unstable runs is the development by the inner fluid of elongated structures which penetrate the outer fluid. These are reminiscent of the fingers associated with the normal Rayleigh-Taylor instability. However, whereas RTI continues until the heavy and light fluids exchange their positions, which is accompanied by their mixing, CFI may terminate earlier, as soon as the generalised Rayleigh discriminant becomes a monotonically increasing function of the radial coordinate, and keep the most inner and outer sections of the initial configuration mostly unaffected.

*Conclusions.* In this letter we have explored the CFI in axisymmetric rotating relativistic and non-relativistic compressible flows. We derived the generalised Rayleigh criterion for CFI in both continuous and discontinuous flows and verified it via axisymmetric computer simulations. However, we have not studied the growth rate of unstable modes in detail. This important issue will have to be addressed in the future.

Due to the imposed symmetry, we could not explore the non-axisymmetric unstable modes of CFI. Interestingly, full 3D simulations of rotating relativistic flows have already been carried out [9, 10] and they do exhibit strong non-axisymmetric modes. However, these modes are interpreted as RT instabilities in rotational motion, while in principle are manifestations of the CFI.

The velocity shear in rotating flows may also be subject to the Kelvin-Helmholtz instability (KHI). As a result of axial symmetry this instability is suppressed in our simulations. The competition between the KHI and CFI is another important topic for future investigations. Finally, the astrophysical jets may include strong magnetic field which may inhibit the growth of CFI and KHI modes and promote current-driven instabilities [5, 11].

## ACKNOWLEDGEMENTS

KNG and SSK were supported by STFC Grant No. ST/N000676/1. The numerical simulations were carried out on the STFC-funded DiRAC I UKMHD Science Consortia machine, hosted as part of and enabled through the ARC HPC resources and support team at the University of Leeds.

---

\* Konstantinos.Gourgouliatos@durham.ac.uk

† S.S.Komissarov@leeds.ac.uk

[1] Bally J., Reipurth B., Davis C. J., 2007, *Protostars and Planets V*, pp 215–230

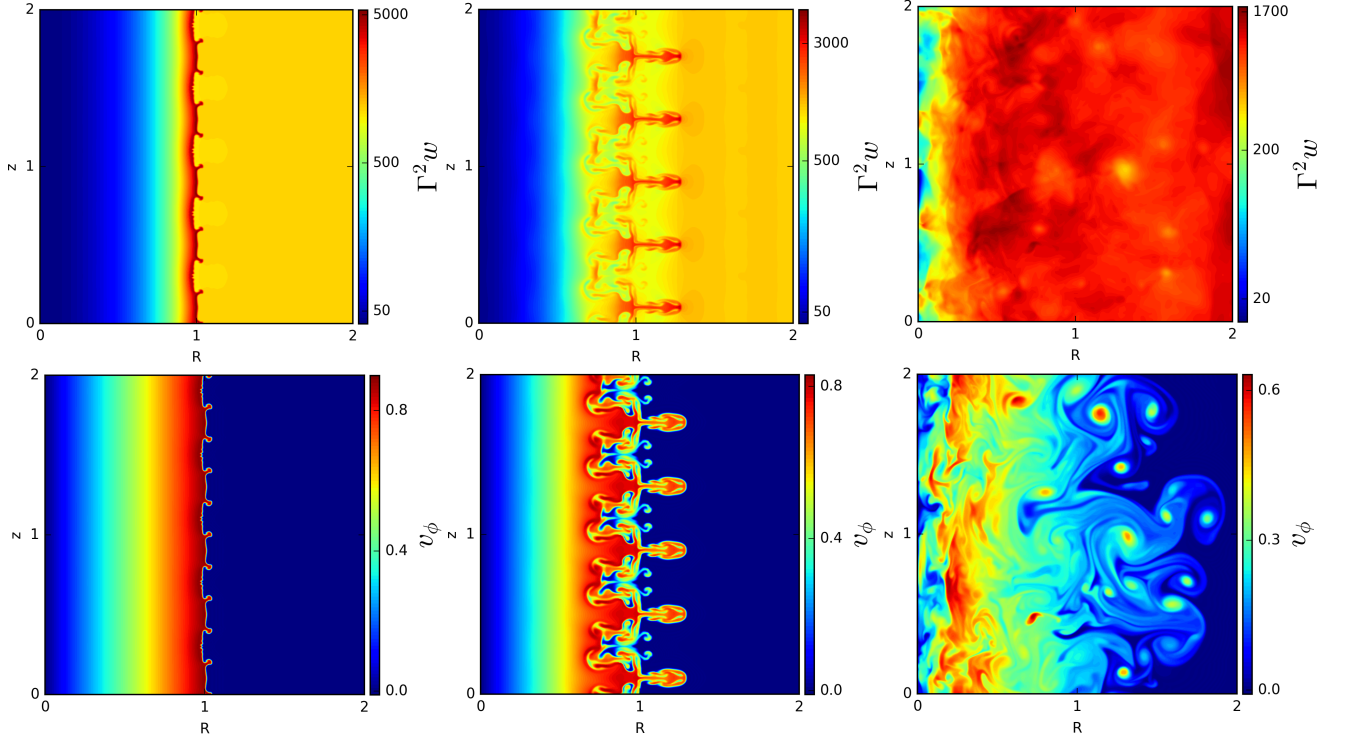


FIG. 1. The distributions of inertial mass density  $\rho_{in} = \Gamma^2 w$  (top row) and  $v_\phi$  (bottom row) for the model R1 at  $t = \pi/2, \pi, 4\pi$  (from left to right).

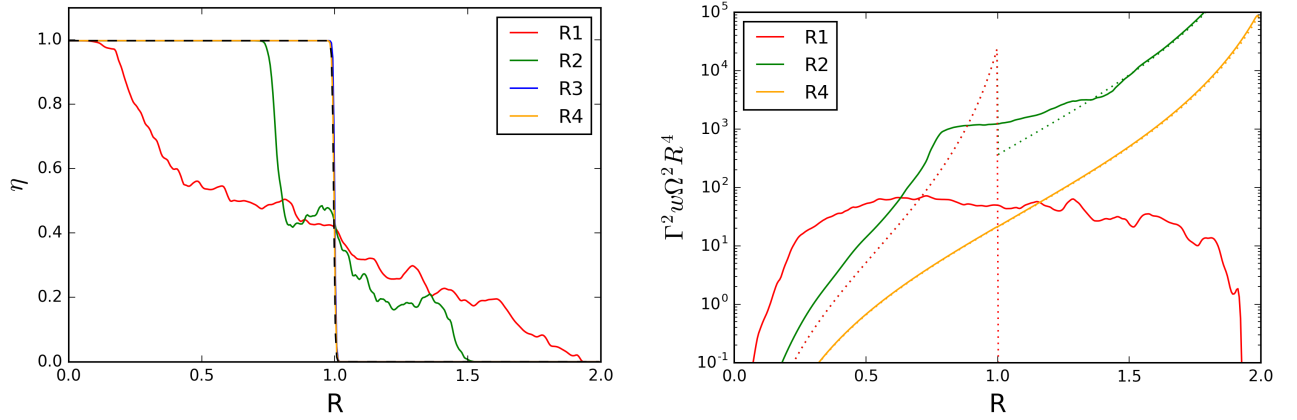


FIG. 2. Left panel: The  $z$ -averaged value of the passive tracer  $\eta$  for unstable relativistic models. The dashed line shows the initial distribution and the solid lines the final distributions (at  $t = 4\pi$ ). The observed spread of the region with  $0 < \eta < 1$  reflects the mixing of the two fluids. Right panel: The  $z$ -averaged generalised Rayleigh discriminant  $\Gamma^2 w \Omega^2 R^4$  for models R1, R2 and R4. The dotted lines show the initial distributions (for R1 it drops to zero at  $R = 1$ ) and the solid lines the final distributions. The instability acts to remove the regions with the negative gradient of the discriminant.

- [2] Bayly B. J., 1988, *Physics of Fluids*, 31, 56
- [3] Bridle A. H., Perley R. A., 1984, *Ann. Rev. Astron. Astroph.*, 22, 319
- [4] Görtler H., 1955, *Zeitschrift Angewandte Mathematik und Mechanik*, 35, 197
- [5] Gourgoullos K. N., Fendt C., Clausen-Brown E., Lyutikov M., 2012, *Mon. Not. Roy. Astron. Soc.*, 419, 3048
- [6] Keppens R., Meliani Z., van Marle A. J., Delmont P., Vlasov A., van der Holst B., 2012, *Journal of Computational Physics*, 231, 718
- [7] Kumar P., Zhang B., 2015, *Phys. Rep.*, 561, 1
- [8] Lee C.-F., Ho P. T. P., Li Z.-Y., Hirano N., Zhang Q., Shang H., 2017, *Nature Astronomy*, 1, 0152
- [9] Meliani Z., Keppens R., 2007, *Astron. Astrophys.*, 467, L41
- [10] Meliani Z., Keppens R., 2009, *Astrophys. J.*, 705, 1594
- [11] Millas D., Keppens R., Meliani Z., 2017, *Mon. Not. Roy. As-*

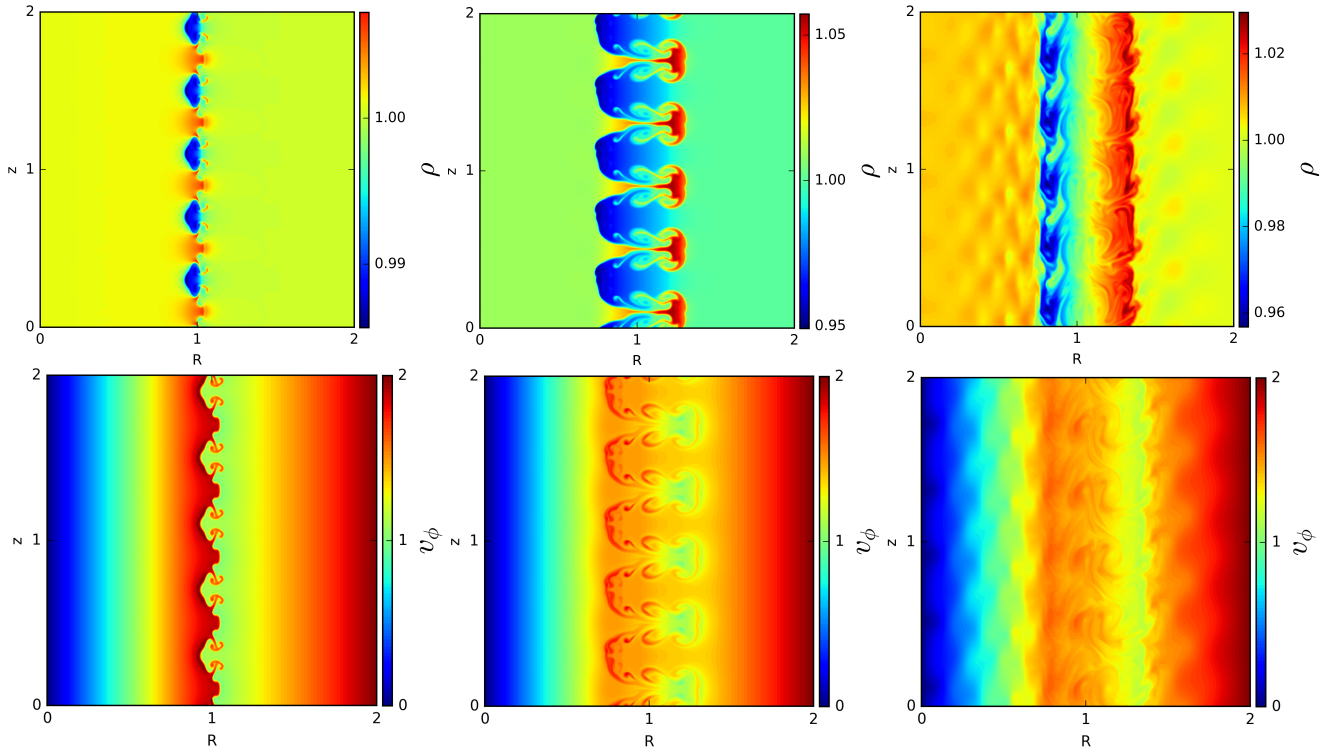


FIG. 3. The distributions of  $\rho$  (top row) and  $v_\phi$  (bottom row) for the model C1 at  $t = \pi/2, \pi, 4\pi$  (from left to right).

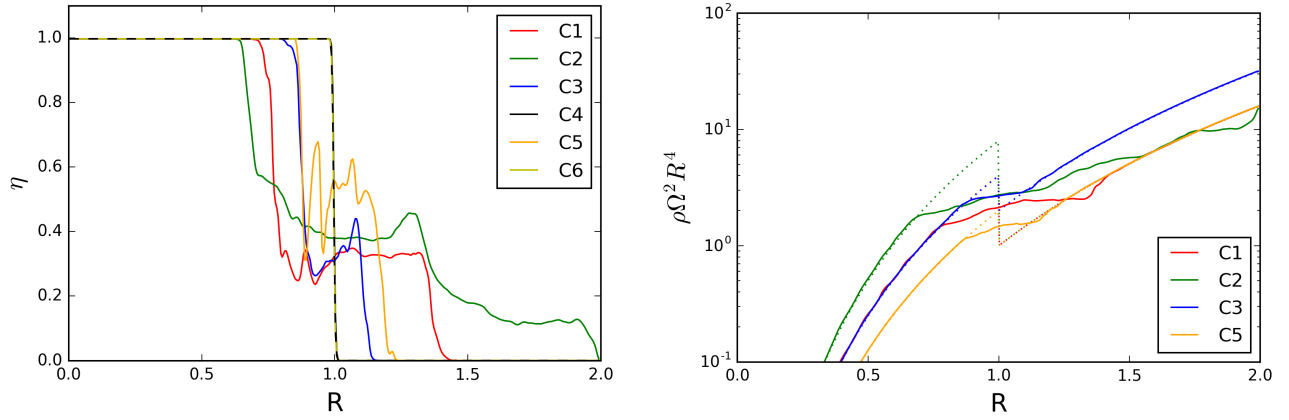


FIG. 4. The same as in Figure 2 but for the Newtonian models.

- tron. Soc. , 470, 592
- [12] Mirabel I. F., 2010, in Belloni T., ed., Lecture Notes in Physics, Berlin Springer Verlag Vol. 794, Lecture Notes in Physics, Berlin Springer Verlag. p. 1 (arXiv:0805.2378), doi:10.1007/978-3-540-76937-8\_1
  - [13] Porth O., Komissarov S. S., 2015, Mon. Not. Roy. Astron. Soc. , 452, 1089
  - [14] Porth O., Xia C., Hendrix T., Moschou S. P., Keppens R., 2014, Astrophys. J. Supp. Ser. , 214, 4
  - [15] Rayleigh L., 1883, Proceedings of the London Mathematical Society, 14, 170
  - [16] Rayleigh L., 1917, Proceedings of the Royal Society of London Series A, 93, 148
  - [17] Sanders R. H., 1983, Astrophys. J., 266, 73
  - [18] Saric W. S., 1994, Annual Review of Fluid Mechanics, 26, 379
  - [19] Taylor G., 1950, Proceedings of the Royal Society of London Series A, 201, 192
  - [20] Zapata L. A., Ho P. T. P., Schilke P., Rodríguez L. F., Menten K., Palau A., Garrod R. T., 2009, Astrophys. J., 698, 1422